Tesla-Range Femtosecond Pulses of Stationary Magnetic Field, Optically Generated at the Nanoscale in a Plasmonic Antenna

Xingyu Yang, Ye Mou, Bruno Gallas, Agnès Maitre, Laurent Coolen, Mathieu Mivelle

Title:

Tesla-Range Femtosecond Pulses of Stationary Magnetic Field, Optically Generated at the Nanoscale in a Plasmonic Antenna

Author list:

Xingyu Yang[†], Ye Mou[†], Bruno Gallas[†], Agnès Maitre[†], Laurent Coolen[†] and Mathieu Mivelle[†,*]

[†]Sorbonne Université, CNRS, Institut des NanoSciences de Paris, INSP, F-75005 Paris, France.
*E-mail: mathieu.mivelle@sorbonne-universite.fr

Abstract:

The inverse Faraday effect allows the generation of stationary magnetic fields through optical excitation only. This light-matter interaction in metals results from creating drift currents *via* non-linear forces that light applies to the conduction electrons. Here, we describe the theory underlying the generation of drift currents in metals, particularly its application to photonic nanostructures using numerical simulations. We demonstrate that a gold photonic nano-antenna, optimized by a genetic algorithm, allows, under high excitation power, to maximize the drift currents and generate a pulse of stationary magnetic fields in the tesla range. This intense magnetic field, confined at the nanoscale and for a few femtoseconds, results from annular optical confinement and not from the creation of a single optical hot spot. Moreover, by controlling the incident polarization state, we demonstrate the orientation control of the created magnetic field and its reversal on demand. Finally, the stationary magnetic field's temporal behavior and the drift currents associated with it reveal the sub-cycle nature of this light-matter interaction. The manipulation of drift currents by a plasmonic nanostructure for the generation of stationary magnetic field pulses find applications in the ultra-fast control of magnetic domains with applications in data storage technologies, but also in research fields such as magnetic trapping, magnetic skyrmion, magnetic circular dichroism, to spin control, spin precession, spin currents, and spin-waves, among others.

Keywords:

ultra-short pulses of magnetic field, plasmonic nano-antennas, genetic optimization, light-matter interactions, inverse Faraday effect

The properties of magnetic fields span orders of magnitudes depending on their source : from thousands of years in geological events such as the reversal of the magnetic poles, down to the femtosecond regime associated with the exchange interaction between spins;[1-2] from Tesla (T) range in the writing head of a hard drive down to few femtotesla in our neurons;[3] from tens of thousands of kilometers in the case of the sun magnetic fields down to sub-nanometer scales in

the case of atoms. However some combinations of these scales are out of reach and to date there is no technological solution for producing intense, confined and ultrafast magnetic fields.

Yet, such a confined, intense and ultrafast field would have profound impacts on magnetism research and technologies related to magnetic fields. For instance, since the pioneer work of Beaurepaire *et al*,[4] researchers have intensively searched for ways to manipulate and study magnetization at the femtosecond timescale using femtosecond lasers,[2] with the aim to control and speed up the current data storage technologies. However, the manipulations of magnetic materials by ultrafast light pulses are still poorly understood.[2, 5-10] As well, the transient processes of magnetic interactions such as spin precession, spin-orbit coupling and exchange interactions take their roots in the femtosecond timescale.[2] The possibility of probing and addressing these different processes and their transient mechanisms using ultrashort pulses of magnetic fields would benefit countless research activities in magnetism: from Zeeman splitting,[11] magnetic trapping,[12] magnetic skyrmion,[13] magneto-plasmonic,[14] ultrafast magnetic modulation,[15] magnetic circular dichroism,[16] to spin control,[17] spin precession,[18] spin currents[19] and spin-waves.[20]

So far, theoretical approaches based on laser-plasma interactions or transient thermoelectric currents in metals have demonstrated interesting results in generating Tesla scale magnetic fields at the nano and picosecond timescales.[21-23] But so far, there are no experimental or theoretical reports on the generation of such an intense magnetic field in the femtosecond timescale.

Alternatively, plasmonic nanostructures have already demonstrated, through the transfer of angular momentum from light helicity to the electron motion, commonly called inverse Faraday effect (IFE),[24-28] the possibility to generate relatively weak stationary magnetic field under certain illumination conditions. In particular, Smolyaninov *et al*. have experimentally shown that circular nano-aperture made in a thin layer of gold could create a magnetic field of a few tens of µT.[29] This study was then followed by several theoretical papers demonstrating similar behavior in plasmonic nanoparticles.[30-31] Although restricted to particles of only a few nanometers and considering only a part of the interactions at these scales, some of these studies have highlighted some quantum aspects of the IFE,[31-32] giving a deeper understanding on these phenomena and this topic. As well, recently, Hsu-Cheng Cheng *et al.* experimentally described how gold nanoparticles in solution under ultrafast excitation generate a stationary magnetic field of a few tens of mT[33] and at subpicosecond timescales, validating the relevance of the plasmonic approach.

However, all these studies have not investigated the femtosecond time behavior of the physical phenomenon involved in the metals considered, *i.e.*, the generation of drift current following the application of an IFE to the conduction electrons, or consider only non-optimized structures, which decrease the potential strength of magnetic field. In order to apply this approach to concrete applications and experiments, it is necessary to develop theoretical and numerical tools allowing the design of complex plasmonic nanostructures able to enhance the IFE to generate strong stationary magnetic fields over nanometric areas and in particular at very short time-scales.

In this letter, we demonstrate that by using a optimization algorithm based on genetic selection, we were able to design a gold plasmonic nanostructure allowing the all-optical generation of femtopulses of stationary magnetic-field, confined at the nanoscale and of the order of the tesla. Specifically, we describe the theory involved in the creation of drift currents in metals solely by optical excitation, and the resulting generation of stationary magnetic fields. We also show that this formalism can be easily used in conjunction with numerical simulations, in our case *via* the finite difference time domain (FDTD) method, allowing the estimation of the stationary magnetic field created for any type of metallic nanostructures. By optimizing a realistic plasmonic nanostructure *via* a genetic algorithm (GA) we have maximized the drift currents in the metal, demonstrating that under a femtosecond (fs) excitation with a peak power of 10^{12} W/cm^2 we could generate a stationary magnetic field (denoted **B** here, as opposed to the magnetic optical field hereafter referred to as **H**) of the order of the tesla, over an area of only a few tens of nanometers in size and for a duration of a few femtoseconds. Moreover, we show that as opposed to most nanoantennas where the optical electric field **E** is focused in a single hot spot, the optimum to generate this intense stationary magnetic field is a structure inducing an annular focusing of the electric field. Likewise, while an azimuthal component of the electric field is required for the creation of the drift currents at the origin of the IFE in the nano-antenna, we show the different contributions of the electric field components at the origin of these currents allowing the generation of the **B**-field, a crucial information for whom wishes to manipulate effectively these currents. Finally, the investigation of the generation of drift currents as a function of time reveals that the temporal mechanisms underlying this light-matter interaction are sub-cycle and occur at twice the frequency of the driving light wave, in good agreement with the non-linear nature of this process.

Results and Discussion:

Drift currents, which represent the slow motion of an electrically charged particle superimposed on a fast motion under the influence of an electromagnetic wave, are well known phenomena in plasma physics.[34] They are much less studied in the nanophotonics community. Yet, drift currents resulting only from an oscillating electromagnetic field, without any contribution of external electric or magnetic fields,[34] are of particular interest in nanophotonics due to the pronounced ability of this research area to manipulate optical fields and field gradients. As described by R. Hertel,[35-36] by considering the free electrons of a metal as a collisionless plasma, the theories of plasma physics can be applied to metals, allowing to describe precisely the creation and the behavior of drift currents. These currents, by their nature, are independent of time and always flow in the same direction, a direction defined by the polarization of light. They can therefore be considered, to a certain extent, as direct currents allowing the generation of stationary magnetic fields. As

demonstrated by R. Hertel *et al* in two successive papers, these drift currents can have two characteristics, one microscopic and relying on the optical electric field,[35] the other macroscopic, resulting from the gradients of optical electric field.[36]

We propose here a simplified description of this theory,[35] whose formalism allows an implementation in common simulation techniques available to the nano-optics community, in order to optimize a plasmonic nanostructure able to significantly increase these optical electric fields and fields gradient leading to the creation of very strong drift current.

It is known that light can apply non-linear forces on moving free charges and in particular electrons.[37] A relevant example is the ponderomotive force[38] used to accelerate charges in a plasma for instance.[39] The time average value of these forces being non-zero, they are at the origin of optically induced drift currents. A way to account for these drift currents is to start from the general equation of a current generated in a metal by an electromagnetic wave $\mathbf{J_\omega}$= e.n.$\mathbf{v}$, where $\mathbf{J_\omega}$ is the conductive current, e the charge of the electron (with e < 0), n the density of free electrons in the metal and $\mathbf{v}$ their velocity. In this paper, all bold characters are vectors. When the free electrons are exposed to an electromagnetic wave, their density can then be written n = <n> + δn, where <n> is the electron density at rest and δn is the oscillating part of n at the angular frequency of the incoming light ω. The current then becomes $\mathbf{J_\omega}$ = e.<n>.$\mathbf{v}$ + e.δn.$\mathbf{v}$, where e.δn.$\mathbf{v}$ can be seen as a perturbation of e.<n>.$\mathbf{v}$. The time average drift current $\mathbf{J_d}$ then corresponds to the non-zero part of the time average <$\mathbf{J_\omega}$> ; $\mathbf{J_d}$ = e.<δn.$\mathbf{v}$>. Hence, by identifying δn and $\mathbf{v}$, it is possible to calculate the drift currents and their associated stationary magnetic fields.

The expression for δn can be extracted from the continuity equation:

$$\frac{\nabla J_\omega}{e} + \frac{\partial n}{\partial t} = 0 \qquad (1)$$

Which can be integrated and rewritten as:[35]

$$n = <n> - \frac{1}{e}\frac{\nabla J_\omega}{i\omega} = <n> + \delta n \qquad (2)$$

The oscillating part of n is then

$$\delta n = -\frac{1}{e}\frac{\nabla J_\omega}{i\omega} \qquad (3)$$

The expression of $\mathbf{v}$, meanwhile, can be obtained directly from the expression of the conduction current which in first approximation is written $\mathbf{J_\omega}$= e.<n>.$\mathbf{v}$, assuming that <n> >> δn.[35]

Hence the velocity is

$$\boldsymbol{v} = \frac{J_\omega}{e<n>} \qquad (4)$$

4

The drift currents in a metal subjected to an electromagnetic wave is then written :

$$J_d = \frac{1}{2e<n>} Re\left(\left(-\frac{\nabla J_\omega}{i\omega}\right) \cdot J_\omega^*\right) \qquad (5)$$

With $J_\omega = \sigma_\omega E$, E being the optical electric field and σ_ω the dynamic conductivity of the metal that can be readily obtained from phenomenological values, $\sigma_\omega = i\omega\varepsilon_0(\varepsilon - 1)$, with ε_0 the dielectric permittivity of vacuum and ε that of the metal.

Therefore, according to Biot and Savart's law, we can deduce the stationary magnetic field generated by these drift currents, induced by light. In this study, only azimuthally polarized drift currents are considered due to the circular symmetry of the structures used. Their radial part does not contribute to the inverse Faraday effect, but would be associated with the ponderomotive force.[35] Therefore, when a reference is made to J_d in this manuscript, it will always be the azimuthal component of the drift currents. We can notice here that the drift current J_d is quadratic regarding the electric field and therefore J_d and B will be linear in terms of optical power. Also, it is known that under high excitation power, the properties of metals can change, due to the creation of hot electrons for example.[40-41] For simplicity, these effects are not considered in this study, a way to include them would be to determine the dielectric permittivity ε of the metal under the influence of these high optical powers.

Following this approach and using Finite Difference Time Domain (FDTD) simulations, we have genetically optimized[42-43] the design of a realistic gold photonic nano-antenna to generate a strong B-field confined to the center of a gold nanostructure (Figure 1a). The antenna consists of a bull-eye shaped structure (Figure 1a) composed of 10 concentric grooves made in a 40 nm gold layer placed on a glass substrate. We chose the smallest width of the grooves to be 6 nm while the largest should be less than 30 nm. Likewise, the width of the metallic rings had to be chosen between 20 and 50 nm. The choice was left to the genetic algorithm to select a nano-aperture or a gold particle in the center of the antenna. We carefully selected these parameters to design a nano-antenna that, for instance, a Helium Focused Ion Beam (He-FIB) could fabricate in a cleanroom facility, both for reasons of etch resolution but also for processing time.[44] A plane wave light pulse with a full-width at half-maximum power temporal duration of 5.3 fs sent from the bottom of the structure (Figure 1a) and with a power density of 10^{12} W/cm^2 excites the antenna. This fluence was chosen because of the resistance of the thin gold layer to these peak powers.[45-46] Nevertheless, it is possible to use even higher powers by inserting the gold nanostructure in a matrix resistant to high energies such as sapphire or glass. This technique could potentially create extremely intense magnetic fields, with the disadvantage of confining it inside the material. We chose the wavelength to be 800 nm and the polarization to be circular and right-handed, this polarization state being

known to generate a strong IFE. Within these constraints, the genetic algorithm was allowed to modify the diameters and sizes of the grooves independently of each other. One of the main difficulty here relates to the fact that in order to calculate the **B**-field generated by the antenna; we need to know the drift current J_d in each metal cell of the FDTD window calculation. Therefore, according to Equation 5, and after a Fourier transformation in order to obtain the continuous wave-like values, the current density J_ω, *i.e.* the optical field **E,** had to be stored in each metal cell of each simulation performed. Moreover, to ensure the robustness of our results and because J_d exists only in the metal, we set the mesh, during the selection process to be 2 nm in the central part of the simulation (*i.e.* where the antenna generates the **B**-field) and then reduced it to 1 nm for fine quantitative study of the optimized structure.

Figure 1b shows the **B**-field generated in the center of the photonic nanostructures (indicated by a blue star in Figure 1a) during the selection process. Each star represents a single simulation and clear evolutionary jumps can be observed during the selection process. The maximum field **B** is found at generation 61 with a value up to 4T.
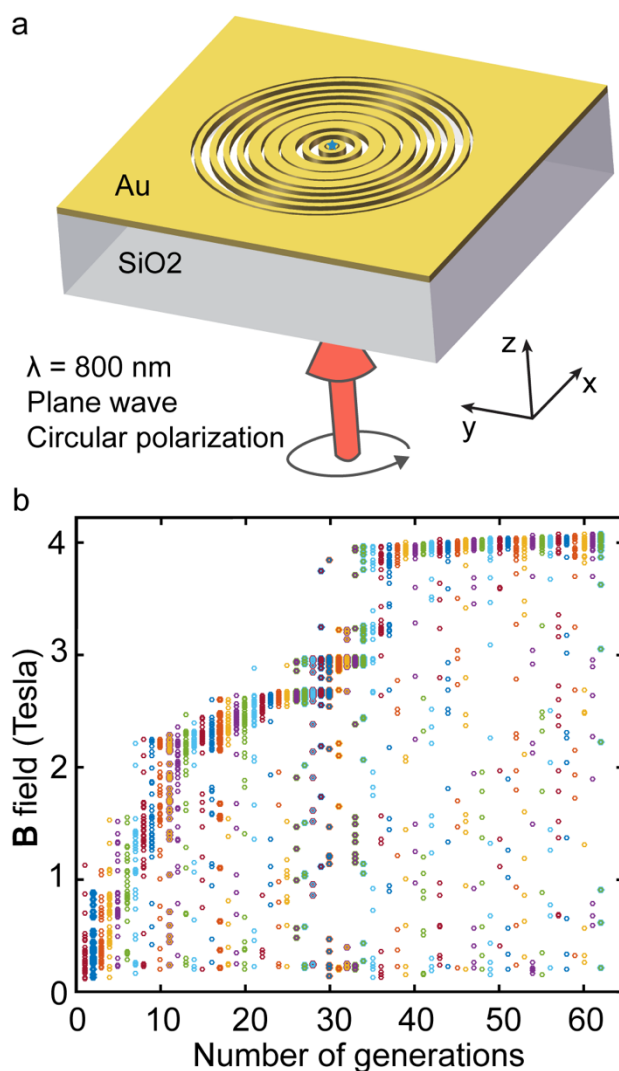
Figure 1. (a) Schematic of the photonic nanoantenna. The antenna consists in a bull-eye structure made of 10 grooves in a 40 nm gold layer deposited on a glass substrate. The excitation is made by plane wave light pulse (5.3 fs) launched from the bottom of the structure. The wavelength is 800 nm and the polarization is circular and right-handed. (b) Amplitude of the magnetic field in the center of the photonic structures during the selection process. Each star corresponds to a single simulation and each generation contains 40 structures.

The geometry of the optimal structure genetically-designed is described in Figures 2a and b. The Table S1 in Supporting Information gives the exact dimensions of the different grooves.

The dimensions given in the Table S1 are accurate to the nanometer, and one could wonder to what extent the intensity of the **B**-field depends on these values. Part of the answer can be found in Figure 1b. Indeed, it can be seen that many different structures during the selection process produced a **B**-field of about 4T, *i.e.* each star around 4T represents a different nano-antenna. The

number of distinct nanostructures producing a **B**-field that is both strong and close to the selected antenna guarantees a fairly weak dependence of the magnetic field with respect to the exact dimensions given in Table S1. Moreover, we have shown in a previous paper[43] that the optimization of a photonic nanostructure by a genetic algorithm depends weakly on the fine structural details. Finally, a similar **B**-field amplitude was found by other genetic evolutions, and the dimensions of the optimized structures were found to be very close to the one presented in this manuscript but not exactly similar (Table S3, Supporting Information). Therefore, it is fair to postulate that these dimensions indicate the type of geometry that allows the creation of a strong stationary magnetic field.

To get an insight into the optical behavior of our optimized structure, Figures 2c and d represent respectively the distribution in the xy plane of the normalized amplitudes of the electric **E** and magnetic **H** optical fields generated in the middle of the metal (in the xz direction) under the excitation conditions described above. It clearly appears that this photonic nano-antenna concentrates the electromagnetic fields in the center of the structure. On the other hand, we can observe that this concentration of electromagnetic energy does not take place at the exact center of the structure, as many nanoantennas are optimized to do, but rather takes the form of an optical electric field ring. The choice having been left to the genetic algorithm to be able to have an aperture or a gold particle in the center of the structure and the fact that the selection process has chosen this distribution of electric field seems to demonstrate the importance of this field distribution for this type of application. Moreover, several genetic optimizations of structures have been conducted and they all show the same electromagnetic distribution (annular) for a structure with an aperture or a gold particle in the center (respectively Figures S1 and S2, Supporting Information). Furthermore, it is important to note different aspects of this structure. The first concerns the size of the central ring where the energy is concentrated. The width of the groove selected by the GA is the smallest possible (6 nm); this is in agreement with the tendency of small gaps to generate strong fields and field gradients, which, in agreement with equation 5, is a determinant element to create strong drift currents[36]. Also, the overall size selected by the GA makes this nano-antenna a resonant structure at 820 nm (Figure S4), very close to the excitation wavelength chosen in this study (800 nm). This result again demonstrates the attractiveness of this algorithmic approach to optimize plasmonic and *a fortiori* photonic resonant nanostructures. Although to be perfectly at resonance, a reduction of the full size of the structure could be considered, indicating that the GA could have done an even finer optimization.
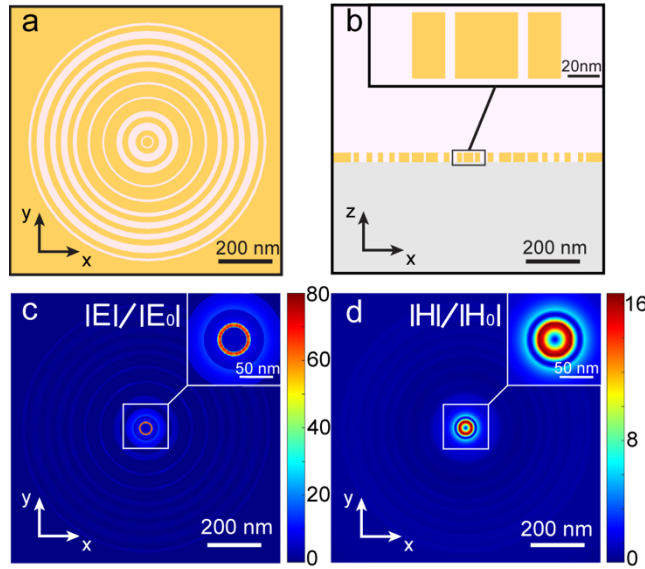
Figure 2. Genetically optimized nano-antenna geometry in (a) an (xy) plane and (b) an (xz) plane. Amplitude distribution in the middle of the antenna in an (xy) plane of (c) the electric E and (d) the magnetic H optical fields, normalized by respectively the electric E_0 and magnetic H_0 optical fields without the photonic antenna.

From this optical electric field distribution, we can then calculate the conduction current density J_ω in the entire structure, and thus using equation 5, calculate the drift current density in each metal cells. Then, using Biot and Savart's law, we can calculate for all points in space the stationary magnetic field **B** generated by this plasmonic nanostructure.

Figure 3a shows the spatial distribution of the **B**-field in an (xz) cross-section in the center of the nanostructure (black rectangle in the inset of Figure 2b). As we can see, the magnetic field is strongly concentrated inside the nanoantenna in a volume of about 50x50x50 nm^3 and in particular inside the metal (symbolized by the white rectangles) with an exponential decay as we move away from the structure. This behavior is directly related to the $1/r^2$ dependence of Biot and Savart's law. Nevertheless, we can notice that the value of the field **B** is still of the order of a Tesla at a distance of about 10 nm from the metal in the z-direction. This range would allow to use this magnetic field in a practical way. Notice that the value of the **B**-field is overall slightly lower than in the selection process (Figure 1b), due to the change in mesh size from 2 to 1 nm, allowing a finer estimation of the   latter.
As well, by observing the orientation of the magnetic field (Figure 3b), it can be seen that the latter shows a solenoid-like behaviour with an orientation mostly perpendicular to the metal surface, upwards, and with field loops around the first metal ring. The complete distributions of the x, y and z components of the **B**-field are shown in Figure S3 (Supporting Information).

Moreover, by changing the polarization from circular right to circular left (Figure 3c), as expected by the inverse Faraday effect, the orientation of the **B**-field is reversed. This result is significant since it demonstrates the tunability of the magnetic field orientation as a function of the excitation polarization and thus its application possibilities. We could mention, for example, the reversal of the permanent magnetization of thin-film.

To this end, the orbital magnetization **M** generated at the center of this structure was calculated *via* equation 6 :

$$M = \frac{1}{2V} \int_V r \times J_d dV \qquad (6)$$

Where V is the volume of the central particle and **r** is the position vector, and was estimated to be equal to 5.27×10^5 A/m.
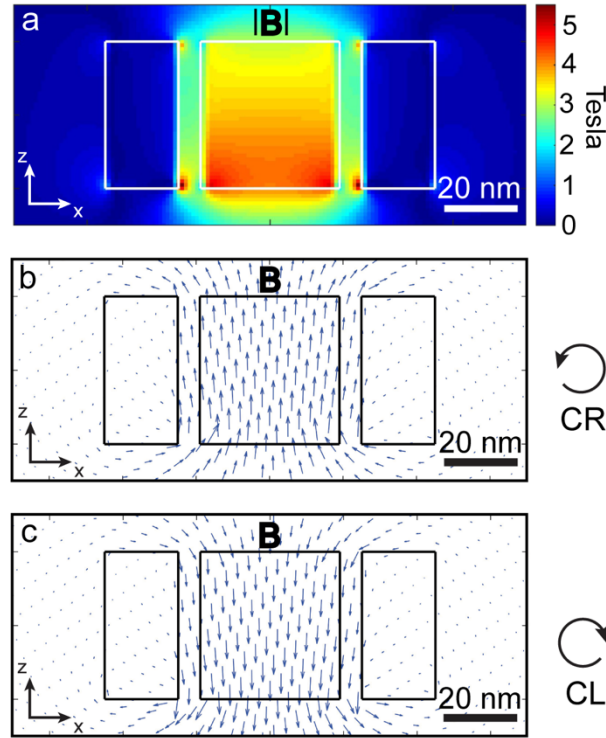

Figure 3. B-field distribution. (a) Distribution of the amplitude of B-field generated at the center of the optimized nanostructure (the metal boundaries are indicated by white rectangles). (b) and (c) B-field vectorial lines for the same area than (a), for (b) a right-handed and (c) left-handed circular polarization. The black rectangles highlight the metal boundaries.

The magnetic field created optically by the nanostructure can only have an intensity of the order of a few teslas at very high optical powers; powers that are accessible to pulsed lasers. However, due to the relaxation time of the electrons in the metal and the relaxing time of the energy stored in the nanostructure itself, the strength of the magnetic field created as well as its temporal behavior are

10

dependent on the characteristics of this pulse. In order to characterize this phenomenon, the temporal response of the **B**-field is studied during the excitation of the nanostructure by the 5.3 fs optical pulse described above.

Figure 4 shows the temporal behavior of the magnetic field created by $\mathbf{J_d}$ together with the light pulse launched in the simulation. First of all, we observe that the electrons' response time delays the magnetic pulse by about 4 fs with respect to the optical pulse. We can then see that the decay of the magnetic pulse is slower than that of the optical pulse due to both the relaxation time of the electrons in gold[47-48] and the relaxation time of the energy within the structure. Finally, while the optical pulse's peak power is the same as during the search for an optimal structure by the genetic algorithm, the magnetic field **B** created by the antenna reaches a value of only about 1.5T. The decay of the optical pulse stops the acceleration of the electrons before reaching their full speed. This phenomenon is explained by the fact that, as opposed to the GA search, the system does not have time to reach a pseudo-permanent regime before the end of the optical pulse; *i.e.*, the nanostructure does not have time to be fully energized before the end of the pulse, allowing it to generate a stronger magnetic field. Therefore, the use of longer pulses would generate higher magnetic fields until saturation, *i.e.*, when the plasmonic nano-antenna is completely energized, around 50 fs, in our case (Figure S5).
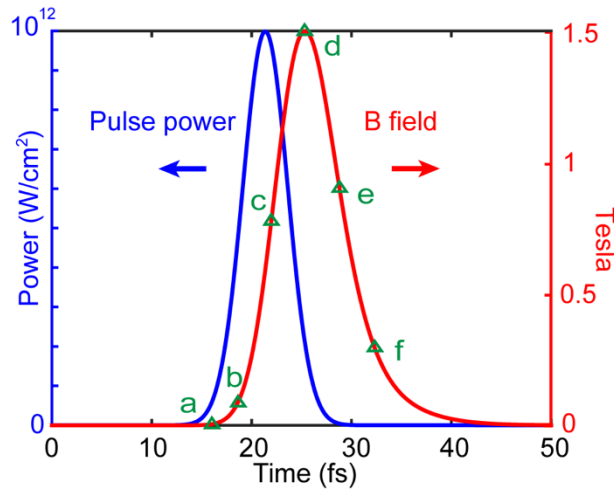
Figure 4. Time evolution of the optical pulse (blue curve) and of the magnetic pulse created by the latter (red curve). The green triangles represent the times at which the B-field distributions in Figure 5 were calculated.

To visualize this delay between optical and magnetic pulses, Figure 5a-f superpose, in an xz plane, the propagation of the electric optical field polarized along y with the magnetic field created by the nanostructure, and this at different times indicated by green triangles in Figure 4. We clearly observe the shift between the optical and magnetic pulses. While the optical pulse is already interacting with the optical nano-antenna (Figure 5b), the **B**-field is still almost zero. On the contrary, when the optical pulse is almost at its minimum (Figure 5d), the **B**-field is maximum. And finally, although the electromagnetic wave has disappeared (Figure 5 e,f) the **B**-field is still very present and decreases slowly due to the dissipation time of the energy within the nanostructure. Note that the magnetic **B**-field distributions shown in Figure 5 correspond to the instantaneous stationary field produced by the drift currents existing in the nanostructure at the time considered. This **B**-field result from two diametrically opposed currents in the nano-antenna, as described hereafter, which rotate around each other, generating a stationary magnetic field in the center of the structure at every instant of the optical pulse.
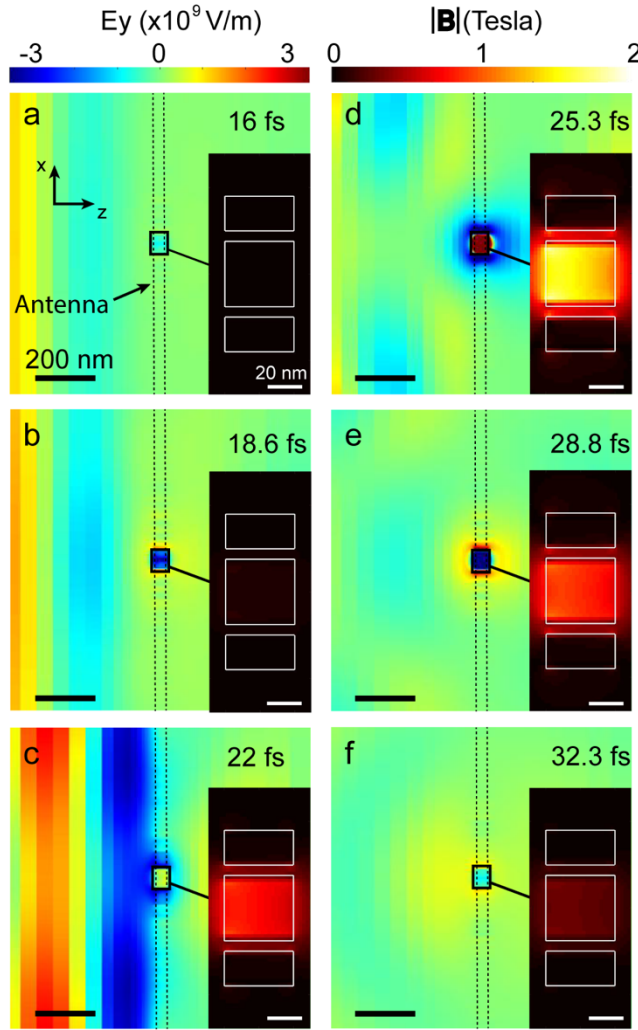
Figure 5. B-field distribution in the xz plane (zoom in inset) created by the optical pulse, together with the y-polarized optical electric field propagating through the simulation window for different times, as indicated in each Figure. These times are also represented on the red curve in Figure 4 by green triangles. The position of the optimized plasmonic antenna in the xz plane is shown by dashed lines.

In order to go further in the understanding of this temporal phenomenon, and in addition to what R. Hertel has demonstrated on long time scales,[36] Figure 6 shows the sub-cycle temporal behavior of drift currents inside the metal (*i.e.* the real part of e.δn.**v**), in the central part of the plasmonic nanostructure, at the location indicated by a green star in inset of Figure 6a. Likewise, the radially and azimuthally polarized electric fields at the same position are also shown in Figure 6a. From this analysis, we can make two major observations. First, the generation of drift currents is in phase with the radially polarized electric field and is 90 degrees out of phase with the azimuthally polarized electric field. Secondly, and in good agreement with the non-linear quadratic process described in equation 5, the temporal dynamics of the J_d currents show behavior that takes place at sub-cycle time-scales. In particular, they are created at twice the frequency of the incident wave, when the

azimuthal electric field is maximum and minimum. This means that two diametrically opposed drift currents co-exist and rotate around each other at each moment in the plasmonic nanostructure (inset in figure 6a), allowing the generation of a stationary magnetic field at any given time of the optical pulse. To better understand the different vectorial contributions of the electric field, and while an azimuthal component of the electric field is required for the creation of the drift currents at the origin of the IFE in the nano-antenna, Figure 6b represents the different contributions of the electric field components in the generation of the drift currents inside the antenna. Figure 6b shows the azimuthally polarized drift currents as a function of the orientation of the electric field considered, at the same position as in Figure 6a. From these results, we can make several observations. First, while the azimuthal drift currents are carried by the azimuthal component of the electric field (right-hand side of equation 5, *i.e.*, in $\mathbf{J}_\omega$), the main contribution to the drift current (left-hand side of equation 5, *i.e.*, in the divergence of $\mathbf{J}_\omega$) comes from the radial polarization of the electric field. This is directly related to the very strong confinement of the field in the first groove of the genetically optimized structure (capacitive effect). Second, the electric field's longitudinal contribution (along Z) has a negative effect on the drift currents, contributing to a decrease in the latter. These results bring a fine understanding of the physical mechanism involved and its temporality, and allows to further manipulate these drift currents. In our opinion, these manipulations allow various applications beyond the simple creation of stationary magnetic fields, such as data processing at time-scales that are also sub-cycle.
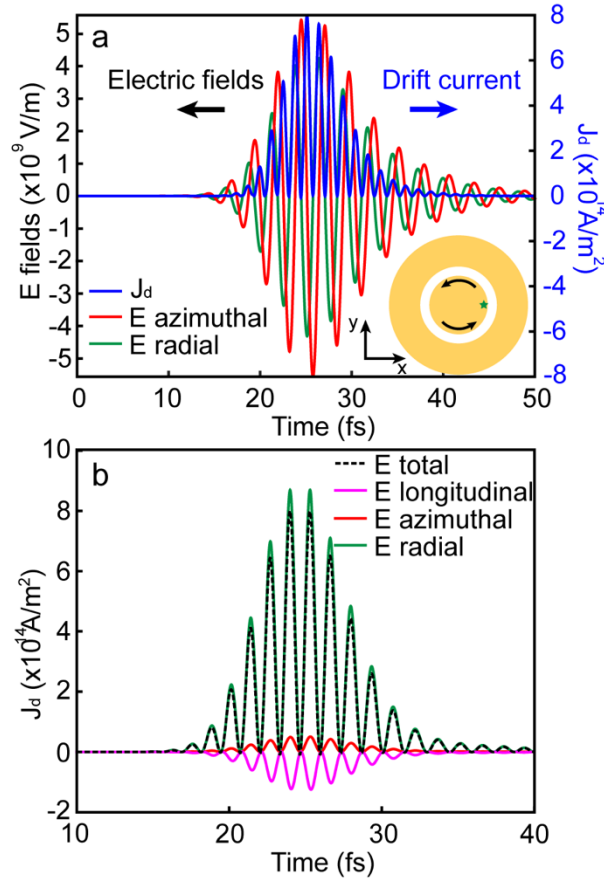
Figure 6. Temporal response of drift currents. (a) Temporal evolution of the drift currents (blue curve), superimposed on the temporal evolution of the radially (green curve) and azimuthally (red curve) polarized electric fields, inside the metal core of the plasmonic nanoantenna, symbolized by the green star in the inset drawing. (b) Contribution of the different components, longitudinal (along Z), azimuthal and radial, of the electric optical field in generating drift currents.

Conclusions:

In conclusion, we have described, *via* a simplified version of the theory describing the creation of drift currents in a metal, the generation of stationary magnetic fields by optical excitation only. We demonstrated that using this formalism, a plasmonic nanostructure optimized by a genetic algorithm could then create stationary magnetic fields in the tesla range under high-power light excitation. This **B**-field is then confined to a region of a few tens of nanometers, mainly oriented out of plane and reversible on demand by switching from right to left circular polarization, thus allowing total control of its out of plane orientation. We have shown that under the influence of a femtosecond optical excitation, a pulse of stationary magnetic field of the order of the tesla is created, on a duration of a few femtoseconds. We have also established that the dynamics and the intensity of the latter is defined by the relaxation time of the electrons and the time needed by the optical nanostructure to dissipate the energy it had stored. Furthermore, we have highlighted the

contribution of the different components of the optical electric field in the generation of azimuthal drift currents in the plasmonic nanostructure, with a significant representation of the radial component, due to a strong capacitive effect in the antenna, allowing a better understanding of the phenomenon to manipulate even further these currents. Finally, we have shown that the dynamics underlying the creation of drift currents is sub-cycle and in particular that their generation takes place at twice the frequency of the incident wave.

Understanding the physical behavior of drift currents inside photonic nanostructures allows us to foresee even more efficient antenna designs for the generation of stationary magnetic fields. In particular, here, only the azimuthal component of $\mathbf{J_d}$ has been used, but one could imagine using all the spatial components of these currents using different antenna designs. Moreover, the generation of stationary magnetic fields is only one of the applications we envision with these currents in metallic nanostructures.

The use of plasmonic nanostructures for all-optical generation of stationary magnetic fields that are altogether confined, intense, switchable on demand, and at the femtosecond timescale represents a turning point for many technological and scientific applications. Among others, we can mention the ultrafast reversal of magnetic thin films for its use in ultrafast data writing, the study of transient magnetic dynamics, nanoscale magnetic resonance experiments, magneto-plasmonics, wave and spin current control.

Methods:

Numerical simulations were conducted using the commercial Lumerical FDTD software.

Each generation of the GA is made up of 40 elements and for each generation, the ten best nanostructures with the highest fitness score, *i.e.* the highest **B**-field, hereafter referred to as "alphas", were mutated or bred into a new generation of 40 elements. Within a new generation, 20 antennas were obtained by mutation of the alphas, with a mutation rate of 10 %, while the breeding of the alphas defined the remaining 20 nanostructures.[42-43, 49]

Associated content:

The Supporting Information is available free of charge at

https://pubs.acs.org/doi/XX.XXXX/acsnano.XXXXXXX.

Exact dimensions of the grooves of the plasmonic nanostructures, two other examples of optimized nanostructures with optical and magnetic behavior, vectorial distribution of the stationary magnetic field, spectral response of the nanostructure optimized by the genetic algorithm, maximum stationary magnetic field reached as a function of the optical pulse duration.

Corresponding author:

Mathieu Mivelle - Sorbonne Université, CNRS, Institut des NanoSciences de Paris, INSP, F-75005 Paris, France.

*E-mail: mathieu.mivelle@sorbonne-universite.fr

ORCID: 0000-0002-0648-7134

Notes:

The authors declare no competing financial interest.

References:

1.   Glatzmaier, G.; Coe, R. Magnetic Polarity Reversals in the Core. In *Treatise On Geophysics*; Schubert, G.; Elsevier: Amsterdam, **2007**; Vol. 8.

2.   Kirilyuk, A.; Kimel, A. V.; Rasing, T., Ultrafast Optical Manipulation of Magnetic Order. *Reviews of Modern Physics.* **2010,** *82*, 2731.

3.   Singh, S. P., Magnetoencephalography: Basic Principles. *Annals of Indian Academy of Neurology.* **2014,** *17*, S107.

4.   Beaurepaire, E.; Merle, J.-C.; Daunois, A.; Bigot, J.-Y., Ultrafast Spin Dynamics in Ferromagnetic Nickel. *Phys. Rev. Lett.* **1996,** *76*, 4250.

5.   Stanciu, C.; Kimel, A.; Hansteen, F.; Tsukamoto, A.; Itoh, A.; Kirilyuk, A.; Rasing, T., Ultrafast Spin Dynamics across Compensation Points in Ferrimagnetic Gdfeco: The Role of Angular Momentum Compensation. *Phys. Rev. B.* **2006,** *73*, 220402.

6.   Koopmans, B.; Malinowski, G.; Dalla Longa, F.; Steiauf, D.; Fähnle, M.; Roth, T.; Cinchetti, M.; Aeschlimann, M., Explaining the Paradoxical Diversity of Ultrafast Laser-Induced Demagnetization. *Nat. Mater.* **2010,** *9*, 259-265.

7.   Radu, I.; Vahaplar, K.; Stamm, C.; Kachel, T.; Pontius, N.; Dürr, H.; Ostler, T.; Barker, J.; Evans, R.; Chantrell, R., Transient Ferromagnetic-Like State Mediating Ultrafast Reversal of Antiferromagnetically Coupled Spins. *Nature.* **2011,** *472*, 205-208.

8.   Graves, C.; Reid, A.; Wang, T.; Wu, B.; De Jong, S.; Vahaplar, K.; Radu, I.; Bernstein, D.; Messerschmidt, M.; Müller, L., Nanoscale Spin Reversal By Non-Local Angular Momentum Transfer Following Ultrafast Laser Excitation in Ferrimagnetic Gdfeco. *Nat. Mater.* **2013,** *12*, 293-298.

9.   Lambert, C.-H.; Mangin, S.; Varaprasad, B. C. S.; Takahashi, Y.; Hehn, M.; Cinchetti, M.; Malinowski, G.; Hono, K.; Fainman, Y.; Aeschlimann, M., All-Optical Control of Ferromagnetic Thin Films and Nanostructures. *Science.* **2014,** *345*, 1337-1340.

10.   Ferrari, E.; Spezzani, C.; Fortuna, F.; Delaunay, R.; Vidal, F.; Nikolov, I.; Cinquegrana, P.; Diviacco, B.; Gauthier, D.; Penco, G. In Element Selective Probe of the Ultra-Fast Magnetic Response to an Element Selective Excitation in Fe-Ni Compounds Using a Two-Color FEL Source, Photonics, Multidisciplinary Digital Publishing Institute: 2017; P 6.

11.   Fu, K.-M. C.; Clark, S. M.; Santori, C.; Stanley, C. R.; Holland, M.; Yamamoto, Y., Ultrafast Control of Donor-Bound Electron Spins with Single Detuned Optical Pulses. *Nat. Phys.* **2008,** *4*, 780-784.

12.   Lu, H.-I.; Kozyryev, I.; Hemmerling, B.; Piskorski, J.; Doyle, J. M., Magnetic Trapping of Molecules *via* Optical Loading and Magnetic Slowing. *Phys. Rev. Lett.* **2014,** *112*, 113006.

13.   Je, S.-G.; Vallobra, P.; Srivastava, T.; Rojas-Sánchez, J.-C.; Pham, T. H.; Hehn, M.; Malinowski, G.; Baraduc, C.; Auffret, S.; Gaudin, G., Creation of Magnetic Skyrmion Bubble Lattices by Ultrafast Laser in Ultrathin Films. *Nano. Lett.* **2018,** *18*, 7362-7371.

14.   Temnov, V. V., Ultrafast Acousto-Magneto-Plasmonics. *Nat. Photonics.* **2012,** *6*, 728.

15.   Ishii, T.; Yamakawa, H.; Kanaki, T.; Miyamoto, T.; Kida, N.; Okamoto, H.; Tanaka, M.; Ohya, S., Ultrafast Magnetization Modulation Induced by the Electric Field Component of a Terahertz Pulse in a Ferromagnetic-Semiconductor Thin Film. *Scientific Reports.* **2018,** *8*, 1-6.

16.   Khorsand, A.; Savoini, M.; Kirilyuk, A.; Kimel, A.; Tsukamoto, A.; Itoh, A.; Rasing, T., Role of Magnetic Circular Dichroism in All-Optical Magnetic Recording. *Phys. Rev. Lett.* **2012,** *108*, 127205.

17.   Fechner, M.; Sukhov, A.; Chotorlishvili, L.; Kenel, C.; Berakdar, J.; Spaldin, N. A., Magnetophononics: Ultrafast Spin Control through the Lattice. *Physical Review Materials.* **2018,** *2*, 064401.

18.   Greilich, A.; Economou, S. E.; Spatzek, S.; Yakovlev, D.; Reuter, D.; Wieck, A.; Reinecke, T.; Bayer, M., Ultrafast Optical Rotations of Electron Spins in Quantum Dots. *Nat. Phys.* **2009,** *5*, 262-266.

19.   Schellekens, A.; Kuiper, K.; De Wit, R.; Koopmans, B., Ultrafast Spin-Transfer Torque Driven by Femtosecond Pulsed-Laser Excitation. *Nat. Commun.* **2014,** *5*, 4333.

20.   Satoh, T.; Terui, Y.; Moriya, R.; Ivanov, B. A.; Ando, K.; Saitoh, E.; Shimura, T.; Kuroda, K., Directional Control of Spin-Wave Emission by Spatially Shaped Light. *Nat. Photonics.* **2012,** *6*, 662-666.

21.   Sandhu, A. S.; Dharmadhikari, A.; Rajeev, P.; Kumar, G. R.; Sengupta, S.; Das, A.; Kaw, P., Laser-Generated Ultrashort Multimegagauss Magnetic Pulses in Plasmas. *Phys. Rev. Lett.* **2002,** *89*, 225002.

22.   Tsiatmas, A.; Atmatzakis, E.; Papasimakis, N.; Fedotov, V.; Luk'yanchuk, B.; Zheludev, N. I.; De Abajo, F. J. G., Optical Generation of Intense Ultrashort Magnetic Pulses at the Nanoscale. *New Journal of Physics.* **2013,** *15*, 113035.

23.   Vienne, G.; Chen, X.; Teh, Y. S.; Ng, Y. J.; Chia, N. O.; Ooi, C. P., Novel Layout of a Bi-Metallic Nanoring for Magnetic Field Pulse Generation from Light. *New Journal of Physics.* **2015,** *17*, 013049.

24.   Van Der Ziel, J.; Pershan, P. S.; Malmstrom, L., Optically-Induced Magnetization Resulting from the Inverse Faraday Effect. *Phys. Rev. Lett.* **1965,** *15*, 190.

25.   Deschamps, J.; Fitaire, M.; Lagoutte, M., Inverse Faraday Effect in a Plasma. *Phys. Rev. Lett.* **1970,** *25*, 1330.

26.   Kurkin, M.; Bakulina, N.; Pisarev, R., Transient Inverse Faraday Effect and Ultrafast Optical Switching of Magnetization. *Phys. Rev. B.* **2008,** *78*, 134430.

27.   Berritta, M.; Mondal, R.; Carva, K.; Oppeneer, P. M., *Ab Initio* Theory of Coherent Laser-Induced Magnetization in Metals. *Phys. Rev. Lett.* **2016,** *117*, 137203.

28.   Kundu, A.; Zhang, S., Effect of Laser Induced Orbital Momentum on Magnetization Switching. *J. Magn. Magn. Mater.* **2018,** *454*, 165-169.

29.   Smolyaninov, I. I.; Davis, C. C.; Smolyaninova, V. N.; Schaefer, D.; Elliott, J.; Zayats, A. V., Plasmon-Induced Magnetization of Metallic Nanostructures. *Phys. Rev. B.* **2005,** *71*, 035425.

30.   Nadarajah, A.; Sheldon, M. T., Optoelectronic Phenomena in Gold Metal Nanostructures Due to the Inverse Faraday Effect. *Opt. Express.* **2017,** *25*, 12753-12764.

31.   Hurst, J.; Oppeneer, P. M.; Manfredi, G.; Hervieux, P.-A., Magnetic Moment Generation in Small Gold Nanoparticles *via* the Plasmonic Inverse Faraday Effect. *Phys. Rev. B.* **2018,** *98*, 134439.

32.   Sinha-Roy, R.; Hurst, J.; Manfredi, G.; Hervieux, P.-A., Driving Orbital Magnetism in Metallic Nanoparticles through Circularly Polarized Light: A Real-Time TDDFT Study. *ACS Photonics.* **2020,** *7*, 2429-2439.

33.   Cheng, O. H.-C.; Son, D. H.; Sheldon, M., Light-Induced Magnetism in Plasmonic Gold Nanoparticles. *Nat. Photonics.* **2020,** *14*, 365-368.

34.   Wolf, R.; Wan, Y.; Xing, X.; Zhang, J. C.; Sazykin, S., Entropy and Plasma Sheet Transport. *Journal of Geophysical Research: Space Physics.* **2009,** *114*.

35.   Hertel, R., Theory of the Inverse Faraday Effect in Metals. *J. Magn. Magn. Mater.* **2006,** *303*, L1-L4.

36.   Hertel, R.; Fähnle, M., Macroscopic Drift Current in the Inverse Faraday Effect. *Phys. Rev. B.* **2015,** *91*, 020411.

37.   Hora, H., Laser Plasma Physics: Forces and the Nonlinearity Principle. Spie Press: Bellingham, **2000**.

38.   Karpman, V.; Shagalov, A., The Ponderomotive Force of a High-Frequency Electromagnetic Field in a Cold Magnetized Plasma. *Journal of Plasma Physics.* **1982,** *27*, 215-224.

39.   Tajima, T.; Dawson, J. M., Laser Electron Accelerator. *Phys. Rev. Lett.* **1979,** *43*, 267.

40.   Labouret, T.; Palpant, B., Nonthermal Model for Ultrafast Laser-Induced Plasma Generation around a Plasmonic Nanorod. *Phys. Rev. B.* **2016,** *94*, 245426.

41.   Hou, X.; Djellali, N.; Palpant, B., Absorption of Ultrashort Laser Pulses By Plasmonic Nanoparticles: Not Necessarily What You Might Think. *ACS Photonics.* **2018,** *5*, 3856-3863.

42.   Feichtner, T.; Selig, O.; Kiunke, M.; Hecht, B., Evolutionary Optimization of Optical Antennas. *Phys. Rev. Lett.* **2012,** *109*, 127701.

43.   Bonod, N.; Bidault, S.; Burr, G. W.; Mivelle, M., Evolutionary Optimization of All-Dielectric Magnetic Nanoantennas. *Advanced Optical Materials.* **2019,** *7*, 1900121.

44.   Kollmann, H.; Piao, X.; Esmann, M.; Becker, S. F.; Hou, D.; Huynh, C.; Kautschor, L.-O.; Bösker, G.; Vieker, H.; Beyer, A., Toward Plasmonics With Nanometer Precision: Nonlinear Optics of Helium-Ion Milled Gold Nanoantennas. *Nano. Lett.* **2014,** *14*, 4778-4784.

45.   Krüger, J.; Dufft, D.; Koter, R.; Hertwig, A., Femtosecond Laser-Induced Damage of Gold Films. *Appl. Surf. Sci.* **2007,** *253*, 7815-7819.

46.   Poole, P.; Trendafilov, S.; Shvets, G.; Smith, D.; Chowdhury, E., Femtosecond Laser Damage Threshold of Pulse Compression Gratings for Petawatt Scale Laser Systems. *Opt. Express.* **2013,** *21*, 26341-26351.

47.   Gall, D., Electron Mean Free Path in Elemental Metals. *J. Appl. Phys.* **2016,** *119*, 085101.

48.   Blanco, M.; Cambronero, F.; Flores-Arias, M. T.; Conejero Jarque, E.; Plaja, L.; Hernández-García, C., Ultraintense Femtosecond Magnetic Nanoprobes Induced by Azimuthally Polarized Laser Beams. *ACS Photonics.* **2018,** *6*, 38-42.

49.   Wiecha, P. R.; Arbouet, A.; Girard, C.; Lecestre, A.; Larrieu, G.; Paillard, V., Evolutionary Multi-Objective Optimization of Colour Pixels Based on Dielectric Nanoantennas. *Nat. Nanotechnol.* **2017,** *12*, 163.

For Table of Contents Only: